Single crystalline $La_{0.5}Sr_{0.5}MnO_3$ microcubes as cathode of solid oxide fuel cell†

Mingjia Zhi,[ab] Guangwen Zhou,[c] Zhanglian Hong,[d] Jin Wang,[ab] Randall Gemmen,[a] Kirk Gerdes,[a] Ayyakkannu Manivannan,[ab] Dongling Ma[e] and Nianqiang Wu*[ab]

Received 22nd July 2010, Accepted 13th September 2010
DOI: 10.1039/c0ee00300j

The efficiency of solid oxide fuel cells (SOFCs) is heavily dependent on the electrocatalytic activity of the cathode toward the oxygen reduction reaction (ORR). In order to achieve better cathode performance, single crystalline $La_{0.5}Sr_{0.5}MnO_3$ (LSM) microcubes with the {200} facets have been synthesized by the hydrothermal method. It is found that the LSM microcubes exhibit lower polarization resistance than the conventional polycrystalline $La_{0.8}Sr_{0.2}MnO_3$ powder in air from 700 °C to 900 °C. The ORR activation energy of the LSM microcubes is lower than that of the conventional powder. The ORR kinetics for the microcubes is limited by the charge transfer step while that for the conventional powder is dominated by the oxygen adsorption and dissociation on the cathode surface.

1. Introduction

The fuel cell is considered as one of the promising technologies to meet the world's ever-increasing demand for clean energy.[1,2] As compared with other types of fuel cells, such as proton exchange membrane (PEM) fuel cell[3,4] and microbial fuel cell,[5] the solid oxide fuel cell (SOFC) is recognized for its high operation temperature, high efficiency and fuel flexibility.[6–8] In the SOFCs with Y_2O_3-stabilized ZrO_2 (YSZ) as the electrolyte, a mixture of Ni with YSZ is often employed as the anode and lanthanum strontium manganite (LSM) as the cathode. Generally the kinetics of the cathodic oxygen reduction reaction (ORR) is much more sluggish than that of the anodic reaction. The efficiency of SOFCs is consequently controlled by the cathodic process. In particular, the ORR on the cathode exhibits significant activation overpotential, especially as the operating temperature of the SOFC is reduced. It is therefore necessary to develop new cathode materials or to modify the architecture of the SOFC cathode in order to improve the kinetics of the ORR. Many methods, including sol–gel,[9,10] molten salt,[11] solid state reaction[12,13] plasma spraying,[14] *etc.*, have been used to synthesize LSM, the state-of-the-art SOFC cathode material. These methods usually lead to polycrystalline powders with random crystalline orientations. It is well known that the electrocatalytic activity of the SOFC cathode is heavily dependent upon the surface chemical properties, such as the oxygen vacancy concentration, the oxygen ion exchange rate as well as the oxygen adsorption and dissociation ability.[15,16] On the other hand, recent studies demonstrate that the catalytic activity of single crystals depend on the specific crystal facet.[17–19] Therefore, the formation of LSM catalysts with controlled shape and external crystal facets is of particular interest. In the present work, single crystalline $La_{0.5}Sr_{0.5}MnO_3$ microcubes with well-defined surface crystal facets are synthesized by hydrothermal processing for use in the SOFC cathode.

[a]*National Energy Technology Laboratory, Department of Energy, 3610 Collins Ferry Road, Morgantown, WV, 26507, USA*
[b]*Department of Mechanical and Aerospace Engineering, West Virginia University, Morgantown, WV, 26506-6106, USA. E-mail: nick.wu@mail.wvu.edu; Fax: +1-(304)-293-6689; Tel: +1-(304)-293-3326*
[c]*Department of Mechanical Engineering, Binghamton University, Binghamton, NY, 13902, USA*
[d]*State Key laboratory of Silicon Materials and Department of Materials Science and Engineering, Zhejiang University, Hangzhou, 310027, P. R. China*
[e]*Institut National de la Recherche Scientifique, INRS-Énergie, Matériaux et Télécommunications, 1650 Boulevard Lionel-Boulet, Varennes, Québec, J3X 1S2, Canada*

† Electronic supplementary information (ESI) available: Fig. S1–S4. See DOI: 10.1039/c0ee00300j

Broader context

A solid oxide fuel cell (SOFC) is an electrochemical device that directly converts chemical energy of fuels to electrical energy. The efficiency of SOFCs is heavily dependent on the electrocatalytic activity of the cathode toward the oxygen reduction reaction (ORR). In order to improve the kinetics of the ORR on the SOFC cathode, single crystalline lanthanum strontium manganite (LSM) microcubes with well-defined surface crystal facets have been developed as the cathode material. Our results have shown that the ORR kinetics for the LSM microcubes is controlled by the charge transfer step while that for the conventional polycrystalline powder is dominated by the oxygen adsorption and dissociation on the cathode surface. The ORR activation energy of the LSM microcubes is lower than that of the conventional polycrystalline powder. Our work has demonstrated that the electrocatalytic activity of the SOFC cathode can be improved by tailoring the surface crystal facet of micro-crystals. The knowledge obtained will facilitate the goal to improve energy efficiency and to reduce emission.

It is generally assumed that the mechanism of the ORR involves several steps, such as oxygen adsorption, dissociation, diffusion and charge transfer.[13,16,20,21] It is unclear which step or steps in the ORR determine the overpotential.[16,22] To the best of our knowledge, there is no study on the ORR of single crystalline LSM microcubes at high temperature, especially at representative SOFC operating conditions. This work presents comparative studies on the ORR processes of both single crystalline LSM microcubes and the conventional LSM powder. Improvement of the SOFC performance by the use of LSM microcubes as the cathode is discussed based on our experimental results.

2. Experimental

2.1 LSM microcube synthesis

The LSM microcubes were synthesized by hydrothermal processing.[23,24] Briefly, 1.5 mmol of $La(NO_3)_3 \cdot 6H_2O$, 1.5 mmol $Sr(NO_3)_2$, 2.1 mmol $Mn(CH_3COO)_2$ and 0.9 mmol of $KMnO_4$ were dissolved into 12 mL deionized water. 0.24 mol KOH was then added to the solution, and be stirred for 1 h. The solution was then loaded into a 25 mL pressure vessel (Parr, 4650) and heated at 240 °C for 24 h. The auto-generated pressure during synthesis was about 15 bar. After naturally cooling down to the room temperature, the black precipitate in the pressure vessel was collected after centrifuging and washing several times with deionized water. Finally the hydrothermal product was dried in an oven at 80 °C for 12 h.

2.2 Material characterization

The morphology of the hydrothermal product was observed by scanning electron microscopy (SEM, Hitachi S-4700). The crystal structure of the as-synthesized sample was characterized by X-ray diffraction (XRD, Panalytical) with a Cu diffractor ($\lambda = 0.15406$ nm) and transmission electron microscopy (TEM, JEOL-2100, operated at 200 kV) with selected area electron diffraction (SAED). The chemical composition and status of the LSM microcubes were analyzed with a PHI Versa Probe 5000 X-ray photoelectron spectroscopy (XPS) with monochromatic Al Kα radiation (1486.6 eV) at an operating power of 25 W.

2.3 SOFC half-cell construction and testing

Electrolyte-supported half cells were used for electrochemical testing. The LSM microcubes were mixed with an ink vehicle (Nextech Materials) at 1 : 2 weight ratio, and then pasted on the YSZ electrolyte disk as the working electrode (WKG). The WKG was sintered at 1100 °C for 3 h. Platinum ink was cast onto the opposite side of the electrolyte disk and sintered at 700 °C for 1 h as the counter (CTR) and the reference electrode (REF). Silver mesh was then attached to the electrodes using the platinum paste to serve as the current collector. The configuration of the SOFC half cell is shown in Fig. S1 in the Supporting Information.† For comparative studies, commercial $La_{0.8}Sr_{0.2}MnO_3$ powder (Nextech Materials) was also tested as a cathode material.

Electrochemical impedance spectra were taken from the three-electrode half cells in the frequency range from 1 MHz to 0.1 Hz at a DC bias of 10 mV at the open circuit condition using Solartron SI 1260 impedance/gain–phase analyzer coupled with Solartron 1287 potentiostat. DC polarization curves were obtained from 0 to −0.5 V at a scan rate of 10 mV s^{-1}. The electrochemical data was processed by the commercial software Zview® and Cview®.

3. Results and discussion

3.1 Microstructure of LSM microcubes

The as-synthesized material exhibited regular cubic morphology (Fig. 1). The size of microcubes ranged from several hundred nanometres to several microns with a median value of about 3 microns. The cubic facets were flat and sharp. In contrast, the commercial LSM powder was composed of irregularly shaped particles with size ranging from 200 nm to 2 μm, as shown in Fig. S2 in the Supporting Information.†

Fig. 2 shows the X-ray diffraction pattern (XRD) of the as-synthesized LSM microcubes, which was assigned to the ABO_3 perovskite structure. The sharp peaks indicate good crystallinity of the microcubes. The peaks corresponding to impurity phases such as $La(OH)_3$ and Mn_2O_3 were not found in the microcubes. TEM was used to further analyze the crystal structure of the LSM cubes. Fig. 3(a) reveals a single cube with a dimension of around 150 nm. Protuberances can be seen on the cube edges, which could be due to the species adsorbed during TEM sample preparation. The sharp SAED pattern in Fig. 3(b) confirms that the cube is a single crystal with a tetragonal structure in the space group *I*4/*mcm*. The lattice parameters derived from the SAED pattern are $a = 5.4$ Å, $b = 5.4$ Å and $c = 7.7$ Å, which are consistent with data reported by others.[25] The external facets of the cube are identified to be {200} from the electron diffraction pattern.

3.2 Electrochemical performance of LSM microcubes

The electrochemical oxygen reduction properties of the LSM microcube electrode were examined at the operation temperatures ranging from 700 °C to 900 °C with an interval of 50 °C. The reaction atmosphere was controlled by mixing 21% of O_2

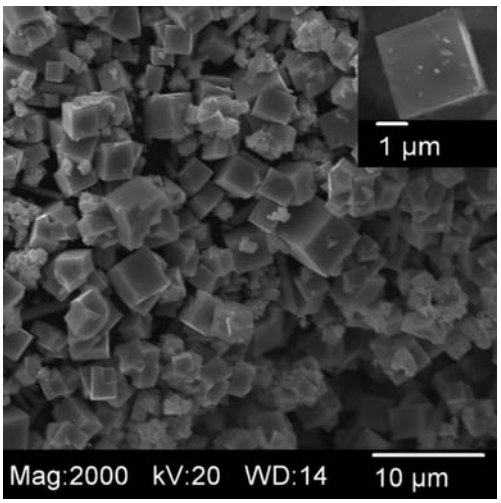

Fig. 1 SEM image of the LSM microcubes; the inset shows a single microcube.

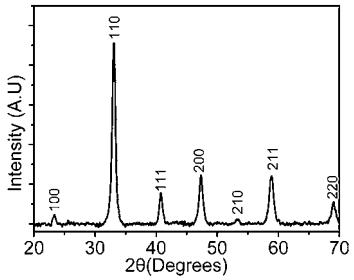

Fig. 2 XRD pattern of the as-synthesized LSM microcubes.

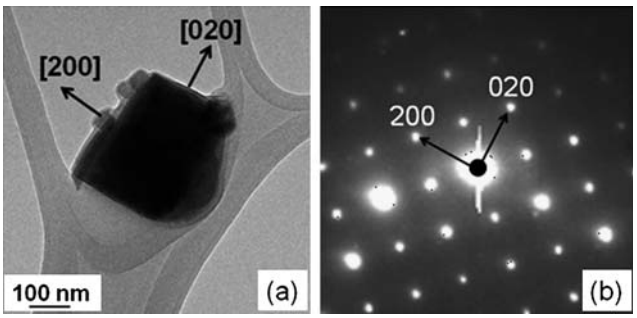

Fig. 3 TEM image of a LSM cube (a), and the SAED pattern (b).

and 79% of N_2 in volume. Nyquist plots of impedance were recorded to investigate the oxygen reduction reaction in the SOFC electrode (Fig. 4). The polarization resistance, R_p, was derived from the high frequency and low frequency intersections with the real axis of impedance. R_p was reduced as the temperature was raised. The polarization resistance was 2.02 Ω cm^2 and 3.21 Ω cm^2 at 850 °C for the LSM microcubes and the conventional powder, respectively. The LSM microcubes exhibited much less polarization resistance (5.32 Ω cm^2) than that (10.37 Ω cm^2) of the conventional powder at 750 °C, which was also better than the data reported in the literature.[26]

To measure the activation energy of the ORR, $\ln(1/R_p)$ was plotted *versus* $1000/T$ (Fig.5), which produces a good linear relationship. The Arrhenius fitting results show that the microcubes have lower activation energy (90.1 kJ mol^{-1}) than the conventional powder (118.6 kJ mol^{-1}). The reported activation energy of the ORR at the LSM/YSZ interface was between 120–200 kJ mol^{-1}.[22,27]

In order to determine the detailed ORR mechanism on the LSM electrode, especially the rate-limiting step, the

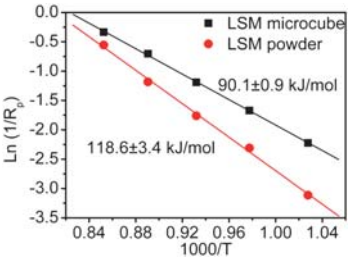

Fig. 5 Arrhenius plots of the LSM electrodes. Note: the activation energy for the oxygen reduction reaction is derived from the slope.

electrochemical performance was investigated by varying the oxygen partial pressure from 5% to 100% at 850 °C. Fig. 6 shows the cathodic Tafel plots of the LSM powder and the microcubes at 850 °C under different O_2 partial pressures. It can be seen that the interval between each curve of the microcubes is smaller than that between the LSM powder curves, which suggests the rate-limiting step in the oxygen reduction processes is different between two materials.

Generally, the oxygen reduction reaction on the LSM electrode can be expressed as[20,28]

$$O_2 + 4e^- + 2V_{\ddot{O}} \rightarrow 2O_O^{\times} \quad (1)$$

where $V_{\ddot{O}}$ represents an oxygen vacancy and $O_O^{\times}$ represents lattice oxygen. A simplified step-by-step reaction pathway is[13]

$$O_2(g) \rightarrow O_{2ad} \quad (2)$$

(molecular oxygen is absorbed on the electrode surface)

$$O_{2ad} \rightarrow 2O_{ad} \quad (3)$$

(molecular oxygen is dissociated to atomic oxygen)

$$O_{ad} \rightarrow O_{TPB} \quad (4)$$

(surface adsorbed atomic oxygen transports to TPB)

$$O_{TPB} + 2e^- + V_{\ddot{O}\ TPB} \rightarrow O_O^{\times} \quad (5)$$

(charge transfer during oxygen reduction at TPB)

Note the electrode used in the experiments was composed of pure LSM. The oxygen reduction reaction should be restricted at the triple-phase boundary (TPB) where all the three phases (*i.e.* oxygen, LSM and YSZ) were present. The dissociated atomic

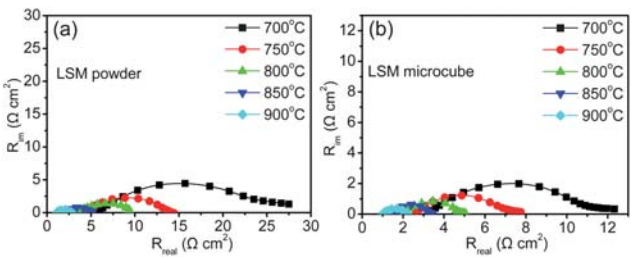

Fig. 4 Impedance spectra of the LSM catalysts taken in air at different temperatures: (a) LSM powder, (b) LSM microcubes.

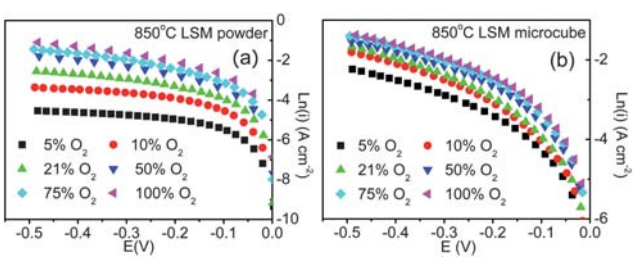

Fig. 6 The cathodic Tafel plots for the LSM electrodes at 850 °C under various O_2 partial pressures: (a) LSM powder, (b) LSM microcubes.

oxygen on the LSM surface migrates to the LSM/YSZ interface, where it is reduced to O^{2-}. If this assumption is correct, it is known that the exchange current density (i_o) and the oxygen content follow an exponential correlation as[20,29]

$$i_o \sim P_{O_2}^m \quad (6)$$

where P_{O_2} is the oxygen partial pressure and the value of m gives the information of the rate-limiting step of oxygen reduction. In general, molecular oxygen adsorption is the rate-limiting step when $m = 1$. Atomic oxygen is involved in the rate-limiting step when $m = 1/2$. Charge transfer is the rate-limiting step when $m = 1/4$ or $-1/4$, depending on the temperature and the oxygen coverage.[20] To determine the value of m, the exchange current densities at various oxygen partial pressures should be measured. According to the Butler-Volmer equation

$$i = i_o \exp\left(\frac{B_a \eta_a F}{RT}\right) - i_o \exp\left(\frac{B_c \eta_c F}{RT}\right) \quad (7)$$

At a high overpotential, it can be simplified as

$$\ln i = -\ln i_o - \frac{B_c \eta_c F}{RT} \quad (8)$$

where i_o is the exchange current density related to the balanced forward and reverse electrode rates at the equilibrium condition. B_a and B_c are the symmetrical coefficients. η_c is the activation polarization, which is the applied cathodic potential. R, T and F are the gas constant, the temperature and the Faraday constant, respectively. Based on eqn (8), the linear region of each Tafel plot at high overpotential was extended to the zero potential and the intercept was taken as the exchange current density (i_o). Fig. 7 shows the dependence of exchange current density on the oxygen partial pressure, which reveals that the m value of the conventional LSM powder was 0.72, close to 3/4. This suggests that both the molecular oxygen adsorption and its dissociation were the rate-limiting steps.[20] In contrast, the m value of the LSM microcubes was 0.30, close to 1/4, which indicates that the charge transfer process was responsible for the rate-limitation in the ORR. It can also be noted that the exchange current density for the LSM microcubes is higher than that for the LSM powder below 75% oxygen partial pressure, which reflects their higher electrochemical catalytic activity toward oxygen reduction at SOFC operation conditions.

The data shown in Fig. 6 and 7 imply that the ORR on the LSM powder is controlled by molecular adsorption and dissociation through the range of pressures tested. However, the exchange current density observed in the LSM powder exceeds that of the LSM microcubes as the oxygen partial pressure approaches 100%. This observation implies that the limitation associated with molecular oxygen adsorption and dissociation on the LSM powder is diminished by elevating the oxygen partial pressure.

It is very important to test the stability of the LSM microcubes as the SOFC cathode at the operating condition. The composite LSM microcube/YSZ (1 : 1 weight ratio) electrode was operated at a DC bias of −0.3 V at 900 °C for 48 h. Fig. S3† shows the chronoamperometric curve. The current was stable with operating time during the experiment, which suggests that the LSM microcubes were thermally stable (Fig. S4†). The morphology and the size of the LSM microcubes were still retained at 900 °C after 48 h of operation. Therefore, the LSM cubes can be potentially used as the SOFC cathode catalyst.

3.3 Surface chemistry of LSM microcubes

To understand the origin of different oxygen reduction behaviors of the LSM powder and the microcube, XPS was used to examine the surface chemistry of the samples. Fig. 8 shows the XPS spectra of the O 1s and Mn 2p core levels obtained from the LSM powder and the microcube, respectively. Oxygen could exist in the LSM catalyst in three forms as reported in the literature.[30,31] The O 1s peak at 529–530 eV can be assigned to lattice oxygen ($O_{lattice}$). The peak at 531.4–531.9 eV is usually related to adsorbed oxygen species (O_{ad}) including O^-, O^{2-} and OH^-, *etc.*, which are believed to be mainly adsorbed on lattice oxygen vacancy sites. The peak around 533 eV is attributed to H_2O molecules adsorbed on the material surface. Therefore, the O 1s core level curves for both the samples can be fitted with three peaks as shown in Table 1. The LSM microcubes possess a higher concentration of adsorbed oxygen species (O_{ad}) compared to the LSM powder, as indicated by the calculated $O_{ad}/O_{lattice}$ ratio. Such adsorbed oxygen species are weakly bonded to the crystal lattice and can be easily released as molecular oxygen between 200–500 °C, leaving the oxygen vacancy sites free.[23] This phenomenon has been confirmed with the TPD (temperature programmed desorption) technique. Previous studies have shown that more oxygen was desorbed between 400 and 500 °C from the LSM microcubes than the LSM nanoparticles.[16] It is therefore believed that the LSM microcubes had more oxygen vacancies on the surface at temperatures above 500 °C under the SOFC operating condition.

The XPS peak of the Mn 2p core level can be deconvoluted to two components.[30] The doublet component at 641.4 eV and

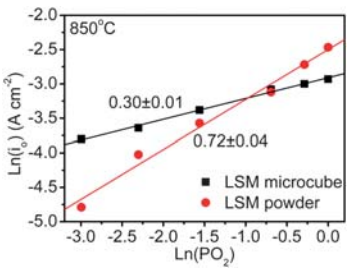

Fig. 7 The relationship of the exchange current density with the O_2 partial pressure.

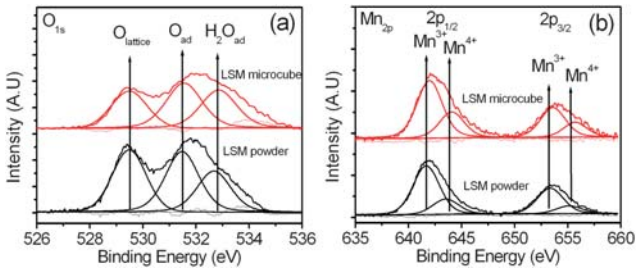

Fig. 8 The XPS spectra of the LSM powder and microcubes; (a) O1s core level, (b) Mn2p core level.

Table 1 Peak fitting results of XPS spectra of the O1s core level

Sample	$O_{lattice}$ peak/eV	O_{ad} peak/eV	H_2O_{ad} peak/eV	$O_{ad}/O_{lattice}$
LSM powder	529.48	531.48	532.67	0.96
LSM microcube	529.50	531.55	532.86	1.32

652.8 eV can be assigned to Mn^{3+} and the doublet at 643.0 eV and 654.3 eV can be ascribed to Mn^{4+}. The intensity ratio of Mn^{4+} to Mn^{3+} is 0.48 and 0.30 for the LSM microcubes and the powder, respectively. The microcube stoichiometry is $La_{0.5}Sr_{0.5}MnO_3$ while the LSM powder stoichiometry is $La_{0.8}Sr_{0.2}MnO_3$. As Sr^{2+} is doped into the A site of the $LaMnO_3$ perovskite, oxygen vacancies are formed to preserve charge balance. The XPS spectrum shift towards Mn^{4+} supports the expectation that LSM microcubes contain more Mn^{4+} cation than the LSM powder. The additional Mn^{4+} promotes formation of the surface oxygen vacancies when Mn^{4+} is converted to Mn^{3+} at relatively high temperatures (above 600 °C), which is accompanied by formation of oxygen vacancies and expressed as[23,30]

$$2Mn^{4+} + O_O^{\times} \rightarrow 2Mn^{3+} + V_{\ddot{O}} + \frac{1}{2}O_2 \quad (9)$$

Such a phenomenon has been confirmed by the TPD experiments, which show a mass decrease corresponding to a gas release at 670 °C.[30] The collective evidence indicates that a greater abundance of Mn^{4+} cations is beneficial for the generation of more oxygen vacancies.

The LSM microcubes have a tetragonal structure and the cube facets are {200} planes that might have a lower oxygen vacancy formation energy than the bulk counterpart. Unfortunately, published evidence was not found in spite of a thorough search. Simulation has shown that the (001) MnO_2-terminated surface is the most stable crystal plane for LSM, and the oxygen vacancy formation energy on this facet is 1.41 eV lower than that of the bulk (6.23 eV *vs.* 7.64 eV).[32,33] The surface vacancy concentration on the (001) MnO_2-terminated surface is found to be $\sim 10^6$ times higher than that of the bulk under the SOFC operating condition.[32]

Considering the above two oxygen vacancy formation processes (O_{ad} release and the Mn^{4+} reduction), one expects that there are more surface oxygen vacancies in the LSM microcubes under the SOFC operating condition. During ORR, the presence of surface oxygen vacancies promotes the dissociative adsorption of oxygen by acting as the active sites, increases the oxygen exchange rate, and favors the migration of the surface oxygen atoms to the triple-phase boundary (TPB).[16,34] Kim *et al.* have found that increasing the concentration of oxygen vacancies can promote the surface diffusion of the O species.[35] Mosleh *et al.* have proposed a mechanism for selective adsorption and dissociation of oxygen molecules on such surface defects and is described below[36]

$$O_2 + V_{\ddot{O}} \rightarrow O_2 \cdots V_{\ddot{O}} \quad (10)$$

$$O_2 \cdots V_{\ddot{O}} + V_{\ddot{O}} \rightarrow 2O \cdots V_{\ddot{O}} \quad (11)$$

where $O_2 \cdots V_{\ddot{O}}$ and $O \cdots V_{\ddot{O}}$ represent the surface oxygen molecules and atoms weakly coupled with the oxygen vacancy, respectively. For the LSM powder, the initial molecular oxygen adsorption and the subsequent dissociation into atomic oxygen are relatively slower. Consequently the ORR kinetics is dominated by these two steps. In contrast, for the LSM microcubes, the oxygen adsorption, dissociation and transport rates are faster on the cubic surface. As a result, more active oxygen species are available at the TPB and subject to reduction, which is reflected by the diminished dependence of exchange current density on the oxygen partial pressure.

4. Conclusions

Single crystalline $La_{0.5}Sr_{0.5}MnO_3$ (LSM) microcubes with {200} facets were synthesized by the hydrothermal method. Their electrochemical oxygen reduction activity was found by half-cell testing to be better than that of the polycrystalline powder in air from 700 °C to 900 °C. Molecular oxygen adsorption and dissociation were the rate-limiting steps during the ORR on the LSM powder cathode, while the charge transfer process was responsible for the rate-limitation in the ORR on the LSM cube cathode. This result is postulated to arise from the superior oxygen adsorption and surface transport rates, which supply an abundance of adsorbed oxygen species to the TPB sites awaiting charge transfer and inclusion into surface vacancies. Our results have shown that the LSM microcubes can be potentially used as SOFC cathode.

Acknowledgements

This work was performed in support of the National Energy Technology Laboratory's research in fuel cells project (41817M2187/41817M2100) under the Research and Development Solutions, LLC (RDS) contract DE-AC26-04NT41817 and West Virginia State Research Challenge Grant-Energy Materials Program (EPS08-01). The facilities and resources used in this work were partially supported by the NSF grant (EPS 0554328) with the matching funds from the West Virginia University Research Corporation and the West Virginia EPSCoR Office.

Notes and references

1 S. G. Chalk and J. F. Miller, *J. Power Sources*, 2006, **159**, 73–80.
2 M. Z. Jacobson, *Energy Environ. Sci.*, 2009, **2**, 148–173.
3 V. Mehta and J. S. Cooper, *J. Power Sources*, 2003, **114**, 32–53.
4 S. Wasmus and A. Kuver, *J. Electrochem. Soc.*, 1999, **461**, 14–31.
5 Y. Qiao, S. J. Bao, C. M. Li, X. Q. Cui, Z. S. Lu and J. Guo, *ACS Nano*, 2008, **2**, 113–119.
6 N. Q. Minh, *J. Am. Ceram. Soc.*, 1993, **76**, 563–588.
7 F. N. Cayan, M. Zhi, S. R. Pakalapati, I. Celik, N. Q. Wu and R. Gemmen, *J. Power Sources*, 2008, **185**, 595–602.
8 M. Zhi, X. Chen, H. Finklea, I. Celik and N. Q. Wu, *J. Power Sources*, 2008, **183**, 485–490.
9 Z. Peng, K. A. Mahone and M. Liu, *J. Mater. Sci. Lett.*, 2000, **19**, 1473–1476.
10 J. Liu, A. C. Co, S. Paulson and V. I. Briss, *Solid State Ionics*, 2006, **177**, 377–387.
11 Y. Tian, D. Chen and X. Jiao, *Chem. Mater.*, 2006, **18**, 6088–6090.
12 M. C. Brant, T. Matencio, L. Dessemond and R. Z. Domingues, *Solid State Ionics*, 2006, **177**, 915–921.
13 J. Kim, G. Kim, J. Moon, Y. Park, W. Lee, K. Kobayashi, M. Nagai and C. Kim, *Solid State Ionics*, 2001, **143**, 379–389.

14 H. Nie, W. Huang, T. Wen, H. Tu and Z. Zhan, *J. Mater. Sci. Lett.*, 2002, **21**, 1951–1593.
15 R. A. D. Souza and J. A. Kilner, *Solid State Ionics*, 1998, **106**, 175–187.
16 S. B. Adler, *Chem. Rev.*, 2004, **104**, 4791–4844.
17 I. Lee, R. Morales, M. A. Albiter and F. Zaera, *Proc. Natl. Acad. Sci. U. S. A.*, 2008, **105**, 15241–14246.
18 N. Tian, Z. Y. Zhou, S. G. Sun, Y. Ding and Z. L. Wang, *Science*, 2007, **316**, 732–735.
19 N. Q. Wu, J. Wang, D. Tafen, H. Wang., J.-G. Zheng, J. P. Lewis, X. Liu, S. S. Leonard and A. Manivannan, *J. Am. Chem. Soc.*, 2010, **132**, 6679–6685.
20 Y. Takeda, R. Kanno, M. Noda, Y. Tomida and O. Yamamoto, *J. Electrochem. Soc.*, 1987, **134**, 2656–2661.
21 O. J. Velle, T. Norby and P. Kofstad, *Solid State Ionics*, 1991, **47**, 161–167.
22 M. J. Jørgensen and M. Mogensen, *J. Electrochem. Soc.*, 2001, **148**, A433–A442.
23 J. Deng, L. Zhang, H. Dai, H. He and C. T. Au, *J. Mol. Catal. A: Chem.*, 2009, **299**, 60–67.
24 C. P. Li, T. Li, B. Wang and H. Yan, *J. Cryst. Growth*, 2006, **295**, 137–140.
25 J. Spooren, R. I. Walton and F. Millange, *J. Mater. Chem.*, 2005, **15**, 1542–1551.
26 S. Z. Wang, X. Y. Liu and M. L. Liu, *J. Solid State Electrochem.*, 2002, **6**, 384–390.
27 J. W. Erning, T. Hauber, U. Stimming and K. Wippermann, *J. Power Sources*, 1996, **61**, 205–211.
28 Y. D. Zhen, J. Li and S. P. Jiang, *J. Power Sources*, 2006, **162**, 1043–1052.
29 J. V. Herle, A. J. McEvoy and K. R. Thampi, *Electrochim. Acta*, 1996, **41**, 1447–1454.
30 F. Teng, S. Liang, B. Gaugeu, R. Zong and Y. Zhu, *J. Catal.*, 2007, **250**, 1–11.
31 N. A. Merino, B. P. Barbero, P. Eloy and L. E. Cadŭs, *Appl. Surf. Sci.*, 2006, **253**, 1489–1493.
32 E. A. Kotomin, Y. A. Mastrikov, E. Heifets and J. Marier, *Phys. Chem. Chem. Phys.*, 2008, **10**, 4644–4649.
33 Y. L. Lee and D. Morgan, *ECS Trans.*, 2009, **25**, 2769–2744.
34 Y. Choi, M. A. Lynch, M. C. Lin and M. Liu, *J. Phys. Chem. C*, 2009, **113**, 7290–7297.
35 J. D. Kim, G. D. Kim, J. W. Moon, Y. Park, W. H. Lee, K. Kobayashi, M. Nagai and C. E. Kim, *Solid State Ionics.*, 2001, **143**, 379–389.
36 M. Mosleh, M. Sogaard and P. V. Hendriksen, *J. Electrochem. Soc.*, 2009, **156**, B441–B457.

Supplementary Material (ESI) for Energy & Environmental Science

Electronic Supplementary Information

Single Crystalline $La_{0.5}Sr_{0.5}MnO_3$ Microcubes as Cathode of Solid Oxide Fuel Cell

Mingjia Zhi[1,2], Guangwen Zhou[3], Zhanglian Hong[4], Jin Wang[1,2], Randall Gemmen[1], Kirk Gerdes[1], Ayyakkannu Manivannan[1,2], Dongling Ma[5] and Nianqiang Wu[1,2],*

[1]National Energy Technology Laboratory, Department of Energy, 3610 Collins Ferry Road, Morgantown, WV, 26507, USA

[2]Department of Mechanical and Aerospace Engineering, West Virginia University, Morgantown, WV, 26506-6106, USA

[3]Department of Mechanical Engineering, Binghamton University, Binghamton, NY, 13902, USA

[4]State Key laboratory of Silicon Materials and Department of Materials Science and Engineering, Zhejiang University, Hangzhou 310027, P. R. China

[5]Institut National de la Recherche Scientifique, INRS-Énergie, Matériaux et Télécommunications, 1650 Boulevard Lionel-Boulet, Varennes, Québec J3X 1S2, Canada

**Corresponding author: E-mail: nick.wu@mail.wvu.edu, Tel: +1-(304)-293-3326, Fax: +1-(304)-293-6689*

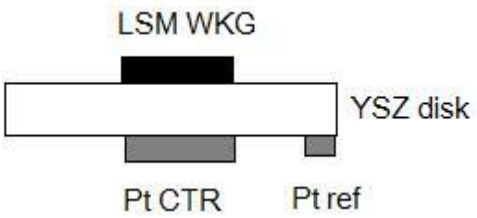

Fig.S1 Schematic illustration of the SOFC half cell

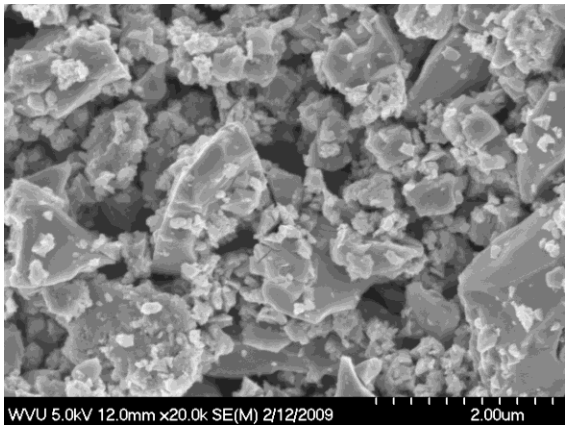

Fig.S2 SEM image of the commercial LSM powder

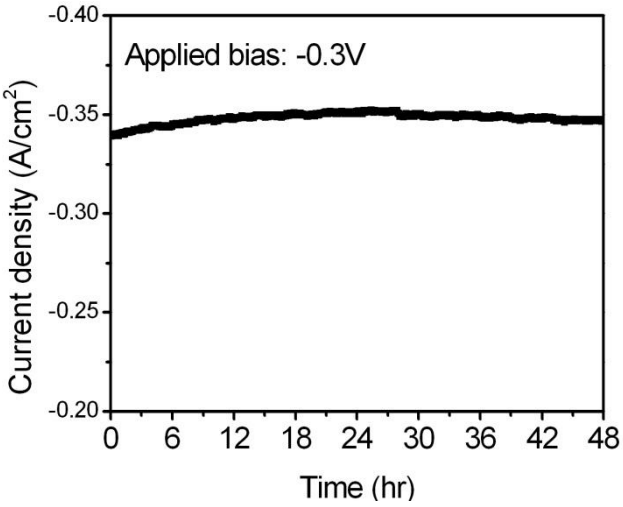

Fig.S3 The electric current density as a function of the operating time for the LSM microcube/YSZ composite electrode at 900 ^{o}C

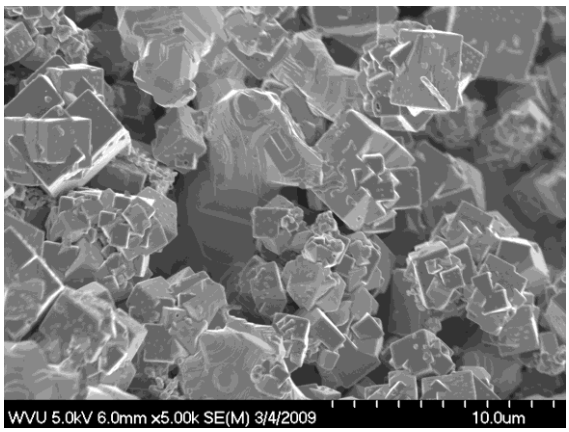

Fig.S4 The morphology of the LSM microcubes after operation at 900 ^{o}C for 48 h